Stability and Nonlinear Evolution of Plasma Clouds via Regularized Contour Dynamics

Edward A. Overman, II, and Norman J. Zabusky
Department of Mathematics, University of Pittsburgh, Pittsburgh, Pennsylvania 15261
(Received 18 July 1980)

A model is introduced of an ionospheric plasma cloud (deformable dielectric) with a piecewise-constant ion density and a *diffusive-regularized boundary*. The linear stability of a single-contour circular cloud is studied and a new evolution equation for modal amplitudes is obtained which has the property that the wave number of maximum amplitude decreases with time (downward cascade). Analytic expressions show that large clouds evolve more slowly and appear more dissipative.

PACS numbers: 52.35.Py, 02.70.+d, 41.10.Dq, 94.30.-d

Ionospheric, collision-dominated, low-β plasma clouds, driven by ambient, uniform electric fields or winds are being studied for two main reasons. First, they are probes of properties of the natural and disturbed ionosphere. Second, they evolve nonlinearly and yield magnetic field-aligned fine-scale structures (irregularities or striations) that can degrade radio-wave propagation.[1]

Past analytic studies of the evolution of ion densities have been almost entirely confined to the linear stability of one-dimensional (1D) stationary states. Linson and Workman,[2] Shiau and Simon,[3] and Völk and Haerendel[4] attributed the cause of striations to the $\vec{E}\times\vec{B}$ gradient-drift instability.[5] Presently there are no 2D stationary states of *continuous* density variation and no 2D stability analyses exist.

In recent computational studies, finite-difference algorithms were used to study the evolution of 1D and 2D ion density clouds with small-amplitude 2D perturbations.[6,7] It has been found that the growth of sinusoidal perturbations on 1D clouds agrees with linear theories.[6] These perturbations evolve into fingerlike striations that emanate from the cloud's "backside" (the direction opposite to the drift velocity $\vec{E}\times\vec{B}/|B|^2$). The results obtained are in qualitative agreement with field experiments.[8]

We now investigate the linear stability of a *two-dimensional* model of an idealized cloud, namely a piecewise-constant distribution of ions:

$$N(x,y,t)=\begin{cases}N_- \text{ for } (x,y)\in D,\\ N_+ \text{ for } (x,y)\notin D,\end{cases} \tag{1}$$

where D is a simply connected, bounded region in R^2 with boundary Γ. The contour, Γ, deforms with a velocity $\vec{V}_d=\vec{E}_-\times\vec{B}/|\vec{B}|^2$, where $\vec{E}_-$ is the self-consistent electric field on the inside of Γ and $\vec{B}=B_0\vec{e}_z$ is Earth's magnetic field, assumed to be constant. In the rest of this paper we set $B_0=1$. Our contributions are twofold: (1) We introduce a contour dynamical model of the piecewise-constant cloud which generalizes the "water-bag" method. The evolution equations include a physically motivated diffusive regularization procedure[9] which inhibits the formation of contour singularities and makes the system *well posed*. (2) We analyze the linear stability of a circular region and demonstrate a new linear phenomenon, "downward cascade," namely, the wave number of maximum amplitude decreases with time. Our work is a combined analytical-numerical study. We also use our results to validate a numerical algorithm which solves the *nonlinear* contour evolution model.

The equations of motion of the continuum ionospheric plasma system of Fig. 1 (inset) have been given as[6]

$$\nabla\cdot(N\nabla\Phi)=0, \tag{2}$$

$$\partial_t N+\vec{V}\cdot\nabla N=\nu\nabla^2 N, \tag{3}$$

$$\vec{v}=-\vec{e}_x\partial_y\Phi+\vec{e}_y\partial_x\Phi, \tag{4}$$

where $\Phi\to -E_0x$ as $|(x,y)|\to\infty$. Here ν is the dissipation parameter (typically very small), E_0 is the ambient electric field, and $\vec{E}=-\nabla\Phi$, where Φ is the potential.

For piecewise constant N, (1), Eq. (2) is equivalent to

$$\begin{aligned}&\nabla^2\Phi_-=0 \text{ for } (x,y)\in D,\\ &\nabla^2\Phi_+=0 \text{ for } (x,y)\notin D,\end{aligned} \tag{5}$$

with the boundary conditions

$$\Phi_+\to -E_0x \text{ as } |(x,y)|\to\infty, \tag{6a}$$

$$\Phi_+=\Phi_-, \text{ and } \partial_n\Phi_+=\lambda\partial_n\Phi_- \text{ on } \Gamma, \tag{6b}$$

where ∂_n is the directional derivative normal to the boundary Γ and $\lambda=N_-/N_+$. These are equivalent to the equations for a dielectric in a uniform electric field. Equations (3) and (4) are equiva-

lent to

$$\partial_t(x, y) = (-\partial_y \Phi_-, \partial_x \Phi_-) + \nu \partial_s{}^2(x, y), \tag{7}$$

for $(x, y) \in \Gamma$, where s is the arc length on Γ. If $\nu = 0$, (7) agrees identically with (3) and (4) for piecewise-constant distributions. For $0 < \nu \ll r_0{}^2\gamma$ [see (14)] the regularization term, $\nu\partial_s{}^2(x, y)$, in (7) is consistent with the dissipative term, $\nu\nabla^2 N$, in (3) for small scale structures to lowest order in ν.[10] Thus, we propose (5), (6), and (7) as a short-time model of a cloud with steep sides.[10]

We now analyze the linear stability of a circular region. It translates downward with a drift velocity $V_d = 2E_0/(\lambda+1)$ associated with the lowest-order internal electric field, E_-. We translate to the (ξ, n) coordinate system, $\xi = x$ and $n = y + V_d t$, and then convert to polar coordinates (r, φ) where φ is the angle measured counterclockwise from the positive n axis. We will solve (5), (6), and (7) on the perturbed boundary

$$R(\varphi, t) = \rho(t) + \epsilon\rho^{(1)}(t) = \rho(t) + \epsilon\left[\alpha_0{}^{(1)}(t) + \sum_{m=1}^{\infty} \alpha_m{}^{(1)}(t)\cos m\varphi\right], \tag{8}$$

where, for convenience, we have assumed the perturbation is symmetric about $\varphi = 0$. From (5) and (6a) we have

$$\Phi_-(r, \varphi) = A_0 + \sum_{m=1}^{\infty} r^m B_m \sin m\varphi, \tag{9}$$

$$\Phi_+(r, \varphi) = E_0 r\sin\varphi + C_0 + \sum_{m=1}^{\infty} r^{-m} D_m \sin m\varphi. \tag{10}$$

Substituting (9) and (10) into (6b) we obtain, to first order,

$$B_m{}^{(1)} = -2[(\lambda-1)/(\lambda+1)^2]E_0\rho^{-m}\alpha_{m+1}{}^{(1)}, \tag{11}$$

for $m \geq 1$. Note that the induction of a dipole field in the first-order solution causes a downshift by one between the Fourier coefficients of the potential $B_m{}^{(1)}$ and the boundary perturbation, $\alpha_{m+1}{}^{(1)}$.

To calculate the time evolution of $\alpha_m{}^{(1)}$ we write (7) in polar coordinates in the translating frame of reference

$$\partial_t R = -R^{-1}(\partial_\varphi \Phi_- + R'\partial_r \Phi_-) + V_d[\cos\varphi + (R'/R)\sin\varphi] - \nu[R^2 + 2(R')^2 - RR'']/R[R^2 + (R')^2], \tag{12}$$

where $R' = \partial R/\partial\varphi$. Substituting (8) in (12), we obtain, to zeroth order,

$$\partial_t \rho = -\nu\rho^{-1},$$

so that

$$\rho = (r_0{}^2 - 2\nu t)^{1/2},$$

where r_0 is the radius of the circle at $t = 0$. To first order,

$$\partial_\tau \alpha_m = m(r_0/\rho)\alpha_{m+1} - Q(m^2-1)(r_0/\rho)^2\alpha_m, \tag{13}$$

where we have suppressed superscripts and where

$$\gamma = 2r_0{}^{-1}E_0(\lambda-1)/(\lambda+1)^2,$$

$$\tau = \gamma t, \quad \text{and } Q = \nu/r_0{}^2\gamma. \tag{14}$$

Thus, *strong* (large λ) *clouds evolve more slowly and appear more dissipative.* We simplify (13) with two nonessential assumptions: First, replace ρ by r_0 since the zeroth-order radius change only weakly affects stability. Secondly, replace $m^2 - 1$ by m^2. We obtain

$$\partial_\tau \alpha_m = m\alpha_{m+1} - Qm^2\alpha_m. \tag{15}$$

If $Q = 0$ and

$$\alpha_m(0) = \delta_{m, m_0}, \tag{16}$$

[so that $R(\varphi, 0) = r_0(1 + \epsilon\cos m_0\varphi)$], then the solution of (15) is

$$\alpha_m(\tau) = \binom{m_0 - 1}{m_0 - m}\tau^{(m_0 - m)}, \quad 1 \leq m \leq m_0. \tag{17}$$

This has the downward-cascade property with the wave number of maximum amplitude being

$$m_{\max} \approx m_0/(1+\tau), \tag{18}$$

at time τ.

Figure 1(a) shows the graph $\alpha_m(\tau)$ vs m of (17) with $m_0 = 40$, and times indicated. We also find that the half-width (width in m at half-amplitude) of (17) increases as

$$\Delta_{1/2} \approx 2(2\ln 2)^{1/2}[m_{\max}(m_0 - m_{\max})/m_0]^{1/2}. \tag{19}$$

$R(\varphi, \tau)$ attains its maximum value $R_{\max}$ when φ

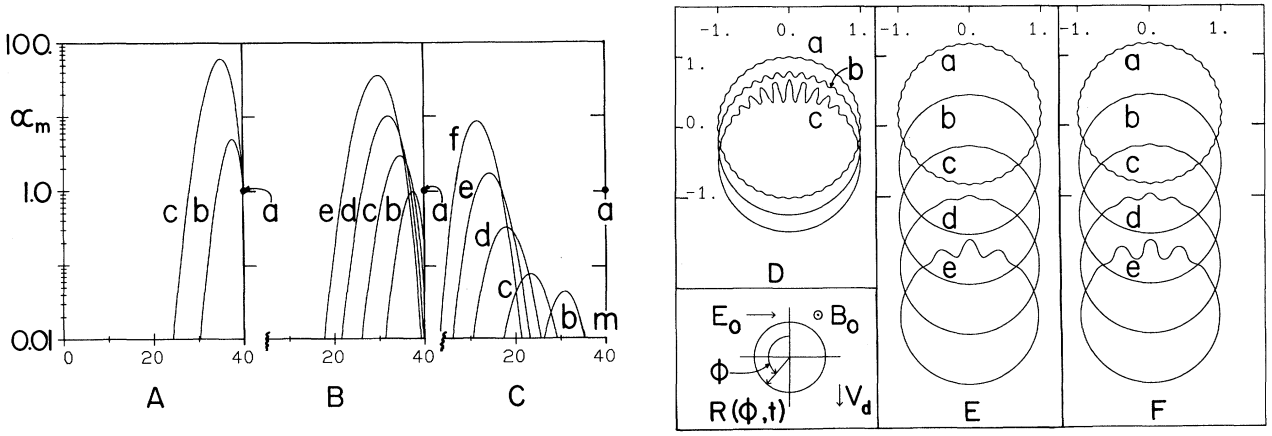

FIG. 1. (a) $\alpha_m(\tau)$ vs m at point a, $\tau=0.0$; curve b, $\tau=0.08$; and curve c, $\tau=0.16$. Solutions of (15) with $r_0=1$, $m_0=40$, $\alpha_{40}(0)=1.0$, $Q=0.0$, and $\lambda=2.0$. (b) $\alpha_m(\tau)$ vs m at point a, $\tau=0.0$; curve b, $\tau=0.08$; curve c, $\tau=0.16$; curve d, $\tau=0.24$; and curve e, $\tau=0.32$. Solutions of (15) with $r_0=1$, $m_0=40$, $\alpha_{40}(0)=1.0$, $Q=0.0135$, and $\lambda=2$. (c) $\alpha_m(\tau)$ vs m at point a, $\tau=0.0$; curve b, $\tau=0.24$; curve c, $\tau=0.48$; curve d, $\tau=0.72$; curve e, $\tau=0.96$; and curve f, $\tau=1.20$. Solutions of (15) with $r_0=1$, $m_0=40$, $\alpha_{40}(0)=1.0$, $Q=0.0315$, and $\lambda=2$. (d) $R(\varphi, t)$ in the laboratory frame at curve a, $\tau=0.0$; curve b, $\tau=0.08$; and curve c, $\tau=0.16$. Solutions of (15) with conditions identical to (b) and with $\epsilon=0.01$. (e) $R(\varphi, t)$ in the laboratory frame at curve a, $\tau=0.0$; curve b, $\tau=0.24$; curve c, $\tau=0.48$; curve d, $\tau=0.72$; and curve e, $\tau=0.96$. Solutions of (15) with conditions identical to (c) and with $\epsilon=0.01$. (f) Solution $R(\varphi, t)$ of the nonlinear equations (5), (6), and (7) for conditions and times identical to (e). Inset: Schematic of circular cloud in the (ξ, n) coordinate system drifting downward with velocity $V_d=2E_0/(1+\lambda)$, where $\lambda=N_-/N_+$.

$=0$, or

$$R_{\max}=r_0+\epsilon\sum_{m=1}^{m_0}\binom{m_0-1}{m_0-m}\tau^{m_0-m}$$
$$=r_0+\epsilon(1+\tau)^{m_0-1}$$
$$\approx r_0+\epsilon\exp[(m_0-1)\tau]. \quad (20)$$

Since α_m is strongly peaked around $m_{\max}(\tau)$, as indicated by (19), the minimum value of R, $R_{\min}$, is attained when $\varphi\approx\pi/m_{\max}$, or $R_{\min}\approx r_0-\epsilon\times\exp[(m_0-1)\tau]$. Thus, the maximum amplitude of the perturbation, $S(\tau)$, is

$$S(\tau)\approx\epsilon\sum_{m=1}^{m_0}\alpha_m(\tau)\approx\epsilon\exp[(m_0-1)\tau].$$

Thus, the dissipationless problem is ill posed.

For $Q>0$, the solution of (15) with the initial condition (16) is

$$\alpha_m(\tau)=[(m_0-1)!/(m-1)!]\sum_{l=m}^{m_0}\left\{\exp(-Qk^2\tau)/\left[\prod_{l=k}^{m_0}Q(l^2-m^2)\right]\right\}. \quad (21)$$

In Fig. 1(b) we show $\alpha_m(\tau)$ with $m_0=40$ and $Q=0.0135$ and in Fig. 1(d) we show the corresponding $R(\varphi, t)$ in the (x, y) laboratory coordinates with $r_0=1$ and $\epsilon=0.01$. In Figs. 1(c) and 1(e) we do the same but for $Q=0.0315$. Note in Fig. 1(b) how α_m increases in time more slowly than in Fig. 1(a). In Fig. 1(c) we see an initial decrease followed by an increase at a much lower wave number. Since (21) is presently rather impenetrable, we convert (15) to a partial differential equation in $\alpha(m, \tau)$ which is easier to analyze. We replace $\alpha_{m+1}(\tau)$ by $\alpha(m, \tau)+\partial_m\alpha(m, \tau)$ and obtain

$$\partial_\tau\alpha=m(\alpha+\partial_m\alpha)-Qm^2\alpha. \quad (22)$$

With the initial condition $\alpha(m, 0)=\exp[-(m-m_0)^2/2l^2]$, we find the maximum growth in amplitude $S\propto\exp[(2Q)^{-1}-1]\tau$ when

$$m_0=(2Q)^{-1}. \quad (23)$$

Figure 1(f) presents a solution of the full nonlinear equations (5), (6), and (7) with initial conditions as in Fig. 1(e). This was obtained with a

regularized contour dynamical algorithm with a node insertion-and-removal algorithm.[11] The close agreement between the linear and nonlinear solutions validates the numerical algorithm.

[1]S. L. Ossakow, Rev. Geophys. Space Phys. 17, 521 (1979).

[2]L. M. Linson and J. B. Workman, J. Geophys. Res. 75, 3211 (1970).

[3]J. N. Shiau and A. Simon, Phys. Rev. Lett. 29, 16–64 (1972).

[4]H. J. Völk and G. Haerendel, J. Geophys. Res. 76, 4541 (1971).

[5]A. Simon, Phys. Fluids 6, 382 (1963).

[6]N. J. Zabusky, J. H. Doles, III, and F. W. Perkins, J. Geophys. Res. 78, 711 (1973). Also, J. H. Doles, III, N. J. Zabusky, and F. W. Perkins, J. Geophys. Res. 81, 5987 (1976).

[7]A. J. Scannapieco, S. L. Ossakow, D. L. Book, B. E. McDonald, and S. R. Goldman, J. Geophys. Res. 79, 2913 (1974). Also, A. J. Scannapieco, S. L. Ossakow, S. R. Goldman, and J. M. Pierre, J. Geophys. Res. 81, 6037 (1976).

[8]N. W. Rosenberg, J. Geophys. Res. 76, 6856 (1971); T. N. Davis, G. J. Romick, E. M. Wescott, R. A. Jeffries, D. M. Kerr, and H. M. Peek, Planet Space Sci. 22, 67 (1974); K. D. Baker and J. C. Ulwick, Geophys. Res. Lett. 5, 723 (1978).

[9]G. I. Marchuk, *Methods of Numerical Mathematics* (Springer-Verlag, New York, 1975), and references therein. See, in particular, 5.2 and 5.3.

[10]N. J. Zabusky and E. A. Overman, II, "Regularization of Contour Dynamical Algorithms" (unpublished).

[11]E. A. Overman, II, and N. J. Zabusky, "A Regularized Contour Dynamical Algorithm for the Evolution of Plasma Clouds and Deformable Dielectrics" (unpublished).

Time-Dependent Images in Transmission Electron Microscopy Associated with the Phase Transitions of $NbSe_3$

K. K. Fung and J. W. Steeds

H. H. Wills Physics Laboratory, University of Bristol, Royal Fort, Bristol BS8 1TL, England

(Received 3 June 1980)

Strandlike domains have been observed in $NbSe_3$ at temperatures below 144 K by imaging in one of the satellite reflections produced by the phase transition. These appear to twinkle rapidly with many strands in the field of view lighting up and switching off in periods of a few seconds. In addition, fringes along these strands have been observed.

PACS numbers: 64.70.Kb, 61.16.Di, 72.15.Nj

The unusual properties associated with the phase transitions of $NbSe_3$ at 144 and 59 K have aroused a great deal of interest.[1] In particular the non-Ohmic electrical conductivity observed near both these transitions has stimulated several investigations[2,3] but still requires a full explanation. The material grows in the form of blade-shaped whiskers with the unique axis (b) of the monoclinic unit cell along the whisker.[4] At each of the phase transitions incommensurate satellites appear in diffraction experiments with wave vector components along the b axis which differ slightly from $\frac{1}{4}b^*$.[5] It is generally accepted that the phase transitions are driven by charge-density-wave (CDW) instabilities and that the non-Ohmic conductivity results from unpinning of the charge density waves.[6] However, direct evidence for the unpinning is at present lacking and the detailed microstructure of the incommensurately modulated state is open to conjecture.

It is the purpose of this communication to report electron microscope observations which may be interpreted as direct evidence for the movement of CDW's and which indicate a stranded nature of the modulated state. These new results permit a reevaluation of a number of previous publications on $NbSe_3$ and lead to a proposal for the nature of the CDW state in this material.

The samples were grown by iodine vapor transport. They have a resistance ratio which is typically about 100:1. Thin foils were prepared from the whiskers for transmission electron microscopy (TEM) by cleavage and they were examined in a Philips EM400 electron microscope with a double-tilting liquid-helium–cooled stage designed by Dr. J. A. Eades and built in this laboratory. The samples were typically 50 nm thick. Temperature control is provided and it is possible to